Electroosmotic Flow in Microchannels with Nanostructures

Takao Yasui,[†,‡,*] Noritada Kaji,[†,‡,#] Mohamad Reza Mohamadi,[§] Yukihiro Okamoto,[‡] Manabu Tokeshi,[†,‡] Yasuhiro Horiike,[⊥] and Yoshinobu Baba[†,∥,*]

[†]Department of Applied Chemistry, Graduate School of Engineering, Nagoya University, Furo-cho, Chikusa-ku, Nagoya 464-8603, Japan, [‡]FIRST Research Center for Innovative Nanobiodevices, Nagoya University, Furo-cho, Chikusa-ku, Nagoya 464-8603, Japan, [§]Physical Chemistry Unit, Laboratory of Macromolecules and Microsystems in Biology and Medicine (MMBM), Curie Institute/CNRS UMR 168/Universite Pierre et Marie Curie, Paris, France, [⊥]National Institute for Materials Science, Tsukuba 305-0044, Japan, and [∥]Health Research Institute, National Institute of Advanced Industrial Science and Technology (AIST), Takamatsu 761-0395, Japan. [#]Present address: Graduate School of Science, ERATO Higashiyama Live-Holonics Project, Nagoya University, Japan.

ABSTRACT Here we report that nanopillar array structures have an intrinsic ability to suppress electroosmotic flow (EOF). Currently using glass chips for electrophoresis requires laborious surface coating to control EOF, which works as a counterflow to the electrophoresis mobility of negatively charged samples such as DNA and sodium dodecyl sulfate (SDS) denatured proteins. Due to the intrinsic ability of the nanopillar array to suppress the EOF, we carried out electrophoresis of SDS−protein complexes in nanopillar chips without adding any reagent to suppress protein adsorption and the EOF. We also show that the EOF profile inside a nanopillar region was deformed to an inverse parabolic flow. We used a combination of EOF measurements and fluorescence observations to compare EOF in microchannel, nanochannel, and nanopillar array chips. Our results of EOF measurements in micro- and nanochannel chips were in complete agreement with the conventional equation of the EOF mobility ($\mu_{\text{EOF-channel}} = \alpha C_i^{-0.5}$, where C_i is the bulk concentration of the *i*-ions and α differs in micro- and nanochannels), whereas EOF in the nanopillar chips did not follow this equation. Therefore we developed a new modified form of the conventional EOF equation, $\mu_{\text{EOF-nanopillar}} \approx \beta[C_i - (C_i^2/N_i)]$, where N_i is the number of sites available to *i*-ions and β differs for each nanopillar chip because of different spacings or patterns, *etc*. The modified equation of the EOF mobility that we proposed here was in good agreement with our experimental results. In this equation, we showed that the charge density of the nanopillar region, that is, the total number of nanopillars inside the microchannel, affected the suppression of EOF, and the arrangement of nanopillars into a tilted or square array had no effect on it.

KEYWORDS: nanostructures · electrophoresis · electroosmotic flow · nanotechnology · nanopillar array

Analytical methods for separation, identification, and detection of a particular molecule from samples with many impurities are of utmost importance in clinical applications and biological industries. Over the past twenty years, capillary and microchip electrophoresis methods have been developed as an alternative platform for the conventional agarose or polyacrylamide gel electrophoresis.[1,2] Capillary and microchip electrophoresis methods mitigate some of the disadvantages of conventional gel electrophoresis, such as its poor resolution and having procedures that are time-intensive and involve manual operations.[3,4] However, in the former electrophoresis methods sieving matrices are still required to achieve size-based separation. The sieving matrices used in capillary or microchip electrophoresis usually consist of randomly networked polymers, and therefore they have an inherent high viscosity. To fill a capillary or microchannel with high-viscosity solution, pressure-driven flow must be used and much time is needed. The process of introducing the sieving matrices into the capillary or microchannel is an intrinsic problem for the integration of total bioanalysis systems.

Since the first report in 1992 on utilizing artificial structures as a matrix for electrophoretic separation of biomolecules by Austin *et al.*,[5] there has been a trend toward switching from randomly ordered polymeric matrices, which involve time-intensive and manual operations,[1−4] to highly ordered sieving structures. Many unique artificial structures, such as micro- and nanopillars,[5−8] nanofilter arrays,[9−12] nanochannels,[13−15] and nanoparticles,[16−20] have been applied for separation of biomolecules. In general, these structures are fabricated inside micro- and nanochannels, and one of the critical issues for electrophoresis of biomolecules in these channels is electroosmotic flow (EOF). EOF has a great influence on the resolution of biomolecular separation, the concentration efficiency of biomolecules, and the sodium dodecyl sulfate (SDS) electrophoresis of proteins in microchannels with nanostructures. In the normal electrophoresis mode, EOF generates a counterflow opposite the electrophoresis migration that can degrade the resolution of separation.[4] Despite efforts that have been focused on the development and application of nanostructures inside a microchannel for electrophoretic separation,[5−18] EOF in

* Address correspondence to yasui.takao@e.mbox.nagoya-u.ac.jp; babaymtt@apchem.nagoya-u.ac.jp.

Received for review April 13, 2011 and accepted September 8, 2011.

Published online September 08, 2011
10.1021/nn2030379

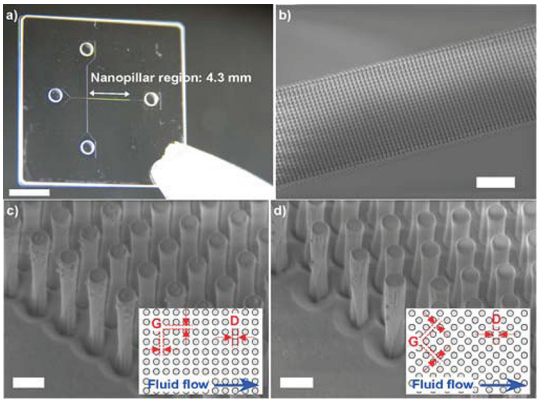

Figure 1. (a) Photo of a nanopillar chip; scale bar, 5 mm. (b) SEM image of the nanopillar array channel; scale bar, 10 μm. This channel is 25 μm wide and 4 μm deep. (c) SEM image obtained at the entrance of the nanopillar region for the square array pattern; scale bar, 1 μm. (d) SEM image obtained at the entrance of the nanopillar region for the tilted array pattern; scale bar, 1 μm. The inserted drawings are a top view of the nanopillars arranged in the (c) square and (d) tilted array patterns. The nanopillars are periodically arranged with various values of the spacing, *G*, ranging from 100 to 1000 nm. The nanopillar diameter, *D*, is 500 nm. In the square array pattern, the adjacent nanopillars are positioned parallel to the flow stream, and in the tilted pattern the close-set positioned nanopillars are inclined 45° to the flow stream.

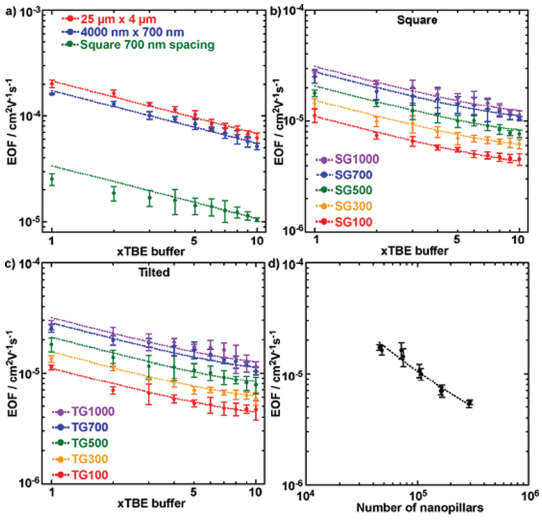

Figure 2. Comparison of EOF in different chips. (a) Logarithmic plot of EOF mobility in the microchannel (red, 25 μm wide and 4 μm deep), nanochannel (blue, 4000 nm wide and 700 nm deep), and nanopillar (green, square pattern with 700 nm spacing) chips. These fitting curves were based on eq 1. (b and c) Logarithmic EOF mobility plots of nanopillar chips arranged in square and tilted array patterns, respectively. These fitting curves were based on eq 2. The designations SG and TG denote the square array and tilted array, respectively. The numbers that follow are the values of the spacing, so 100 means "with 100 nm spacing". (d) Dependence of EOF mobility on the number of nanopillars in the channel; this plot of the EOF mobility of 5× TBE was extracted from panels (b) and (c). The inserted fitting curve in (d) was based on an inverted square root of the number of nanopillars, (number of nanopillars)$^{-0.5}$. Error bars show the standard deviation for a series of measurements (N = 5).

channels with nanostructures has been little studied.

EOF occurs upon applying an external electric field parallel to the solid surface of micro- or nanochannels that include an electrolyte solution. EOF also occurs where an interfacial charge forms in the fluid near the surface. EOF is known to be a surface-driven flow, and therefore it should not depend on the size or shape of the channels, but rather on the charge distribution around several tens of nanometers from the surface of the channels. In quartz (fused silica) chips this interfacial charge may arise because of silanol group deprotonation at a silica−water interface. This phenomenon results in a net negative charge to the silica surface, and positive counterions are attracted to the surface to satisfy the condition of electrical neutrality. Subsequently an electric double layer (EDL) is formed near the interface. EDLs provide several benefits such as the following: when an external electric field is applied, the mobile charges in the double layer are moved toward the cathode, and through viscous coupling with the uncharged fluid, most of the solution is dragged in a uniform plug-like flow;[21] when an electric field is applied to nanochannels under the condition that the EDLs are overlapping inside the nanochannels, both positively and negatively charged ions are enriched at the cathode end and depleted from the anode end;[22] under low salt conditions, ion transport inside the nanochannel is controlled by transport of counterions accumulated onto the charged channel walls;[23] and concentration polarization near the nanochannel is initiated with perm-selective nanochannels.[24] Understanding EDLs is also of significant importance in electrochemistry, because they also affect the behavior of ions at several tens of nanometers from the electrodes.[21−24] However, it is extremely difficult to measure ion movement in EDLs directly. In the present study, we measured EOF in microchannels with nanostructures as a comprehensive approach to understand EDLs, because the EOF is generated by EDLs when electric fields are applied. We fabricated nanopillar array structures on quartz chips (Figure 1) with various spacings between the nanopillars in tilted and square array patterns. Using these nanopillar chips, we made a quantitative evaluation of EOF around nanopillars, which led us to propose a new modified equation that can explain the correlation of EOF in nanopillar chips and the charge density of the nanopillar region or the total number of nanopillars inside the microchannel. Finally, we apply our nanopillar chips for SDS electrophoresis of proteins.

RESULTS AND DISCUSSION

EOF Measurement. First, our intention was to define the effects of nanopillars and their patterns on EOF in microchannels. Figure 1b shows an SEM image of closely packed nanopillars inside a 25 μm wide microchannel. These nanopillars of 500 nm pillar

diameter (D) had a 4 μm height and therefore a high aspect ratio of about 8. We fabricated two types of nanopillar arrays in the channel, square and tilted array patterns. In the square array pattern (Figure 1c), nanopillars were positioned parallel to the microchannel with homogeneous pillar spacing (G) ranging from 100 to 1000 nm. In the tilted array pattern (Figure 1d), the nanopillars were precisely set with 45° inclination to the fluid flow and G was also set from 100 to 1000 nm. The SEM images of nanopillar chips with different pillar spacing are shown in the Supporting Information.

After fabrication of the chips we measured EOF in different chips. Figure 2a shows logarithmic plots of the EOF mobility against the concentration of TBE buffer (tris-borate-EDTA) in different chip types; compared to the pillar-free chips, EOF in nanopillar chips with 700 nm spacing was efficiently suppressed. For instance EOF mobility (5× TBE) in the microchannel (25 μm × 4 μm) without nanopillars was ~1.0×10^{-4} cm^2 V^{-1} s^{-1}, while inside the nanopillar region with 700 nm spacing, the EOF decreased by 1 order of magnitude (1.0×10^{-5} cm^2 V^{-1} s^{-1}).

Two possible effects could be involved in suppression of EOF in nanopillar chips. The first could be the effect of the spatial size, which is expressed here as nanopillar spacing G and nanopillar height (4 μm). There have been several reports on scaling down the spatial size, and it was shown that the viscosity of water increases as spatial size approaches a nanoscale.[25,26] The second could be the effect of a characteristic of the nanopillar array, such as its higher surface-to-volume ratio than pillar-free micro- and nanochannels. To verify which of these two plays the more important role in suppression of EOF in nanopillar chips, first we fabricated a nanochannel 700 nm deep and 4 μm wide; these dimensions were comparable to those of a nanopillar chip with 700 nm spacing and 4 μm height. The results in Figure 2a (blue) show that EOF mobility in the nanochannel was relatively lower than in the microchannel but higher than in the nanopillar chip. Using a simplified version of the Smoluchowski equation for EOF,[3] we interpreted the lower EOF in the nanochannel compared to the microchannel:

$$\mu_{\text{EOF-channel}} = \frac{4\pi\sigma}{\kappa\eta} = \alpha C_i^{-0.5} \qquad (1)$$

where η is the viscosity of the solvent, κ^{-1} is the Debye length, σ is the net charge of the channel walls, C_i is the bulk concentration of the i-ions, and α is a constant that differs in micro- and nanochannels. The fitting curves in Figure 2a that are based on eq 1 are in a good correlation with our experimental results in the micro- and nanochannels. We extracted α from the lines in Figure 2a and found that for the microchannel (25 μm wide and 4 μm deep) chip, α was 2.15×10^{-4}, and for the nanochannel (4 μm wide and 700 nm deep) chip, it was 1.74×10^{-4}. The difference in α was $\alpha_{\text{microchannel}} = 1.24\alpha_{\text{nanochannel}}$. Considering that in eq 1 $4\pi\sigma$ is constant, κ^{-1} is a function of $C_i^{-0.5}$, and the only variable is α, which is inversely proportional to the viscosity of the solvent, we concluded the first effect was plausible; the factor $x \propto \eta \propto \alpha^{-1}$, which is related to the viscosity of buffer in the nanochannel, was 1.24 times higher than that in the microchannel ($x_{\text{nanochannel}} = 1.24x_{\text{microchannel}}$). For instance, the spin−lattice relaxation time for water in the ^{1}H NMR spectrum, $1/T_1$, reported by Tsukahara *et al.*[26] was in good agreement with our results ($1/T_{1\text{nanochannel}} = 1.25 \times 1/T_{1\text{microchannel}}$). Another possibility for the effect was Joule heating during the experiment. The viscosity of water changes rather quickly as a function of temperature, and the temperature of water would be affected by Joule heating during the experiment. In order to evaluate the influence of the temperature changes by Joule heating, we used a fluorescent dye (rhodamine B) in 5 × TBE buffer[27−29] as a temperature indicator at 25 °C. The difference of normalized fluorescence intensity between micro- and nanochannels was less than 0.01%, and therefore we concluded that the effect of Joule heating on the viscosity of water in our channels was negligible.

However we found that in nanopillar chips (Figure 2a) the EOF mobility in low buffer concentrations from 1× to 4× TBE exhibited an aberration from the fitting curve obtained using eq 1, which we showed had worked well with micro- and nanochannels. Also, despite the comparable spatial sizes, the EOF mobility in the nanopillar chips with 700 nm spacing was lower than that in the 700 nm nanochannel. To elucidate these counterintuitive results, we needed to reconsider the charge density in eq 1. In our experiments, the overlap of EDLs could be negligible because EDLs were estimated from eq S5 to be around 3 nm. The charge density inside the nanopillar region is the sum of the average charge density in a single nanopillar, and therefore the EOF mobility in nanopillar chips can be expressed as (see the Supporting Information)

$$\mu_{\text{EOF-nanopillar}} = \int \mathbf{n}_j \, d\mathbf{n}_j \frac{2\sigma}{\kappa'\eta a}$$

$$\approx \beta\left(C_i - \frac{C_i^2}{N_i}\right)^{-0.5} \qquad (2)$$

where $\mathbf{n}$ represents lattice vectors of the array and the location of the nanopillars in the lattice, a is the distance representing the limits within which no other ions can approach the channel wall, κ' is defined in eq S18, σ is the net charge of the nanopillar, N_i is the number of sites available to i-ions, and β is a constant that differs among nanopillar chips (different spacings or arrays). This modified EOF equation (eq 2) could predict the aberration of EOF in nanopillar chips from the conventional equation at low buffer concentrations

TABLE 1. Constant β, Which Differs among Nanopillar Chips (different spacings or arrays) in eq 2, Surface-to-Volume (S/V) Ratios, and the Cylindrical Pores of Diameter R Were Replaced by $4/R$ on the Basis of the Surface-to-Volume Ratio

		nanopillar spacing/nm				
		100	300	500	700	1000
β ($\times 10^{-5}$)	square	1.08	1.51	2.04	2.74	3.06
	tilted	1.09	1.52	2.06	2.78	3.10
S/V	square	0.0102	0.0042	0.0026	0.0019	0.0014
	titled	0.0093	0.0035	0.0020	0.0013	0.0008
R/nm	square	389	962	1566	2155	2956
	tilted	428	1138	2031	3089	4944

(less than 4× TBE buffer here). To further investigate the proposed modified equation, we measured the EOF mobility in nanopillar chips with five spacings using several concentrations of TBE buffer (Figure 2b and c). There were no noticeable differences between square (2b) and tilted array (2c) patterns in the nanopillar chips. With both nanopillar patterns, the EOF mobility decreased as the concentration of TBE buffer increased. All the fitting curves based on eq 2 showed good correspondence to the experimental results in nanopillar chips. We extracted N_i from the lines in Figure 2b and c, and we found that for the nanopillar chips in square and tilted array patterns N_i was 25, which means *i*-ions could approach a nanopillar at intervals of 62.8 nm. We also extracted β from the lines in Figure 2b and c and summarized these values in Table 1. By calculating the viscosity of buffer in nanopillar chips with cylindrical pores of diameter R, the smallest R in the nanopillar chips increased the viscosity of buffer only 2.8 times compared to that in bulk,[26] and therefore, the difference in β was affected by not only the viscosity of buffer but also the combination of the lattice vectors and viscosity of buffer. Another conclusion here was that the EOF suppression in nanopillar chips depended on the charge density inside the nanopillar region and, therefore, the total number of nanopillars. To confirm the dependence of the total number of nanopillars on the EOF suppression, the EOF mobility in 5× TBE buffer was plotted against the total number of nanopillars in Figure 2d. The results showed good agreement with our assumption, and actually, the fitting curve was inversely proportional to the square root of the number of nanopillars.

In Figure 3 we used an indirect method to visualize the EOF in the nanopillar chip. In the indirect method, fluorescein was electrically driven from the cathode to the anode against the EOF. As seen in Figure 3a, in the pillar-free microchannel (25 μm wide and 4 μm deep) the EOF profile was for plug flow, in agreement with previous results.[30] However the EOF profiles in the nanopillar chips were inverse parabolic flow (Figure 3b–e). Schematic representations of EOF

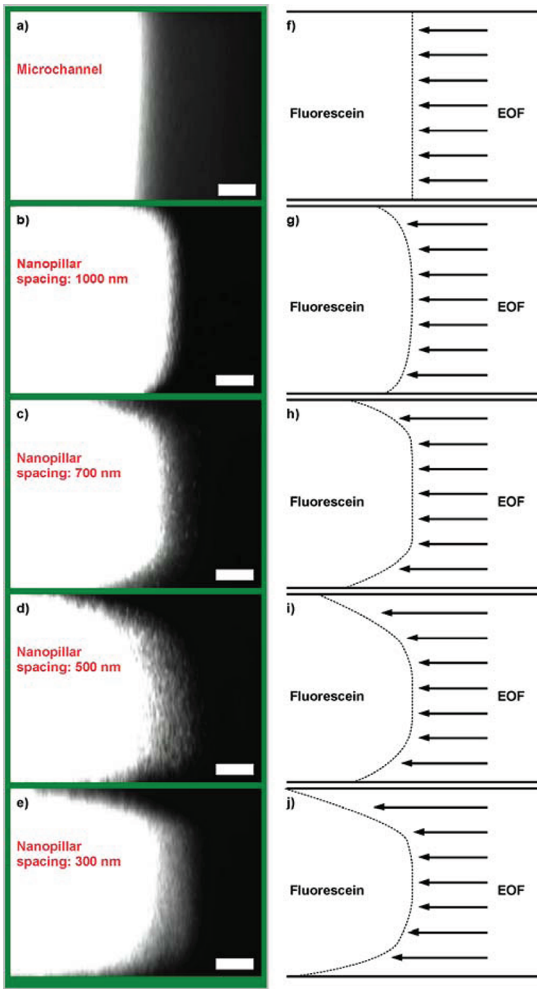

Figure 3. EOF profiles and sketches. (a–e) EOF profiles. (f–j) Sketches of EOF profiles. (a and f) Microchannel. (b–e and g–j) Nanopillar array channels with spacing of (b and g) 1000, (c and h) 700, (d and i) 500, and (e and j) 300 nm. The scale bars are 5 μm. The fluorescein flow was from the left, and the EOF was from the right.

profiles in Figure 3f–j showed that as the nanopillar spacing decreased or the number of nanopillars increased, the EOF profile was more and more deformed.

Separation of SDS–Protein Complexes. To verify the intrinsic ability of EOF suppression in nanopillar chips, we applied nanopillar chips to separate SDS–protein complexes. Generally, adding SDS to electrophoresis buffer in microchannels increases the EOF mobility, so we first studied the effect of SDS on EOF in nanopillar chips. The results in Figure 4a showed that the EOF mobility in quartz and PMMA (poly(methyl methacrylate)) channel chips was almost the same ($\sim 1.0 \times 10^{-4}$ cm^2 V^{-1} s^{-1}); however, the EOF mobility in the tilted pattern nanopillar chips with 100 nm spacing was smaller than that in the PMMA microchannel chips filled with 5% polyacrylamide (MW: 600 000–1 000 000). Adding 0.1 wt % SDS to the electrophoresis buffer increased the EOF mobility in the PMMA microchannel filled with 5% polyacrylamide by 1 order of magnitude.

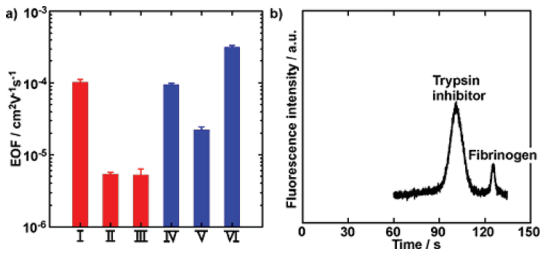

Figure 4. EOF mobility and separation results. (a) Semilogarithmic plot of EOF mobility in the nanopillar array channel and PMMA microchannel chips (I: quartz microchannel; II and III: nanopillar chips arranged in the tilted array pattern with 100 nm spacing; IV, V, and VI: PMMA microchannel). I, II, and IV were acquired in 5× TBE buffer ($N = 5$). III was acquired in 5× TBE buffer with addition of 0.1 wt % SDS ($N = 5$). V was acquired in 5× TBE buffer with 5% polyacrylamide ($N = 5$). VI was acquired in 5× TBE buffer with 5% polyacrylamide and addition of 0.1 wt % SDS ($N = 5$). (b) Separation results of fibrinogen and trypsin inhibitor. An electric field of 70 V/cm was applied for the separation.

Such a high EOF, which is a counterflow to the electrophoretic mobility of the SDS−protein complexes was reported to hinder the separation of SDS−protein complexes in uncoated PMMA chips.[31] However, in nanopillar chips, adding 0.1 wt % SDS did not change the EOF mobility due to electrostatic repulsion between the quartz surface and the SDS molecules. Once we had seen that SDS had no effect on EOF mobility in nanopillar chips, we applied the nanopillar chips for separation of SDS−protein complexes. The separation of two SDS−protein complexes in the tilted array pattern nanopillar chip with 100 nm spacing was achieved within 150 s with an applied electric field of 70 V/cm (Figure 4b). These results demonstrated the feasibility of nanopillar chips for separation of biomolecules without any sieving gel or polymers and without any surface coating.

CONCLUSION

In conclusion, the results reported in this paper are the first for a quantitative investigation and formulation of EOF mobility in microchannels with nanostructures. We also demonstrated that the EOF suppression by nanopillar array structures was attributable to a function of the total number of nanopillars, *i.e.*, the charge density, inside the microchannel, and therefore, our modified equation could predict the EOF mobility. Finally we applied nanopillar chips for troublesome separation of SDS−protein complexes without any surface coating. To the best of our knowledge, our report is the first quantitative investigation of electrochemistry in a microchannel with nanostructures. Our results should widen the application fields for electrophoretic devices due to precise control of the EOF and also should give new insight into the behavior of ions in EDLs.

METHODS

Nanopillar Chip Fabrication. Nanopillar chips were made on a quartz substrate using electron beam lithography (EBL), photolithography, and reactive ion etching, as described elsewhere.[7] Briefly, a 20 nm thick Pt/Cr layer was sputtered on a 0.5 mm thick quartz substrate. A positive electron beam (EB) resist (ZEP-520A, ZEON) was coated onto the substrate to a thickness of about 1 μm by a spinner. Then, nanopillar array patterns were delineated by EBL (ELS-7500, Elionix), which made nanoholes of 500 nm diameter and 1 μm depth. Ni was electroplated into the nanoholes in the EB resist to get a strong mask resistant to reactive ion etching. An array of Ni posts was formed after removal of the EB resist, and then the quartz substrate was covered with a positive photoresist (OFPR8600, Tokyo Ohka Kogyo). Standard photolithography was used to pattern 25 μm wide features. Neutral loop discharge plasma etching was applied to the substrate, in which case the Ni posts and photoresist were a mask for the CF_4 etching. Inside the 25 μm wide microchannel, nanopillars were formed of 500 nm diameter and 4 μm height, arranged with various spacings from 100 to 1000 nm. Reservoirs were formed by punching with an ultrasonic drill, followed by removal of the mask and the metal layer. The quartz substrate was bonded to a 130 μm thick quartz cover plate by dipping both of them briefly into H_2SiF_6 and then removing and bonding them at 5 MPa and 65 °C for 12 h (Figure S2).

EOF Measurement. Tris-borate-EDTA (TBE) buffer was used to measure the EOF mobility. The number in front of the × shows the dilution ratio from 10× TBE, which consisted of 890 mM tris-borate and 20 mM EDTA. In the PMMA microchannel, 10% polyacrylamide (MW 600 000−1 000 000) solution in water (lot #586810, Polyscience, Inc.) was added to 10× TBE buffer, so the final concentration of polyacrylamide was 5% in 5× TBE buffer. To examine the effect of sodium dodecyl sulfate addition, 10% SDS (Fluka) was added to the buffer solution up to 0.1 wt % SDS.

The EOF mobility in nanopillar chips was measured using the current monitoring method[32] to avoid considering different electrical resistances that would be derived from a number of nanopillar arrays, complicating our problem. As shown in Figure S3a and b, there were four reservoirs in the nanopillar chip. In the measurement, the microchannel with nanopillars and three reservoirs were filled with a buffer (*e.g.*, 5× TBE), and the fourth reservoir was filled with a 5-fold dilution buffer (*e.g.*, 1× TBE). A high-voltage power supply (HVS448, LabSmith) was used to provide high voltage during the measurements through platinum electrodes, which were precisely positioned on an inverted microscope (Eclipse TE-300, Nikon), and current variation was recorded every 50 μs using a PC and the Sequence software program (LabSmith). Figure S3c presents the measured current (red line) as a function of time when one reservoir was filled with 1× TBE buffer and other reservoirs were filled with 5× TBE buffer, and there were a microchannel (L = 9.025 mm) and a nanopillar region. The current fell as the 5× TBE buffer was replaced continuously with the 1× TBE buffer inside the microchannel and nanopillar region. This current drop continued until the entire microchannel and nanopillar region became filled with the 1× TBE buffer. The measured current data were approximated to the smoothed data (blue line). Smoothing was carried out using the partial least-squares method in Kaleidagraph (Synergy software). The smoothed result showed an appropriate curve at the center of the data points. Comparing the partial least-squares method with the standard least-squares one, the former could include most of the outliers, and therefore the smoothed data had good reliability. The time interval Δt is the time required to complete the filling of the 1× TBE buffer inside the microchannel and nanopillar region

by the EOF (Figure S3d). The EOF flow velocity was calculated in $L/\Delta t$ with a known length of L.

To measure relative temperature changes, we used 10 μM rhodamine B (Sigma-Aldrich, Inc.) in 5× TBE, which was introduced into the microchannel and the nanochannel while applying a high voltage for 80 s. To observe EOF profiles indirectly, 30 μM fluorescein (Fluka) in 2× TBE buffer was introduced into the microchannel with the nanopillars also by applying a high voltage. An extra high pressure mercury lamp (HB-10103 AF, Nikon) was used as an optical source to illuminate fluorescein flow, and emitted fluorescence images were obtained with an EB-CCD camera (C7190-43, Hamamatsu Photonics K.K., Hamamatsu) through a 40×/0.75 NA objective lens (Nikon). All images were recorded on a DV tape (DSR-11, Sony) and captured by image capture software (Adobe Premiere 6.0, Adobe).

Acknowledgment. This research is partially supported by the Japan Society for the Promotion of Science (JSPS) through its "Funding Program for World-Leading Innovative R&D on Science and Technology (FIRST Program)" and the Grant-in-Aid for JSPS Fellows. We also thank Dr. R. Ogawa and Dr. S. Hashioka for their technical support.

Supporting Information Available: (1) SEM images, (2) fabrication process, (3) EOF measurement, (4) EOF in the net nanopillar region, (5) equations in nanopillar chips, (6) EOF profile in a nanochannel, and (7) SDS−protein complexes. This material is available free of charge *via* the Internet at http://pubs.acs.org.

REFERENCES AND NOTES

1. Rickwood, D.; Hames, B. D. *Gel Electrophoresis of Nucleic Acids: A Practical Approach*, 2nd ed.; Oxford: New York, 1990.
2. Watson, J. D.; Baker, T. A.; Bell, S. P.; Gann, A.; Levine, M.; Losick, R. *Molecular Biology of the Gene*, 5th ed.; Cold Spring Harbor Laboratory Press: San Francisco, 2004.
3. Landers, J. P. *Handbook of Capillary Electrophoresis and Associated Microtechniques*, 3rd ed.; CRC Press: New York, 2008.
4. Viovy, J. L. Electrophoresis of DNA and Other Polyelectrolytes: Physical Mechanisms. *Rev. Mod. Phys.* **2000**, *72*, 813–872.
5. Volkmuth, W. D.; Austin, R. H. DNA Electrophoresis in Microlithographic Arrays. *Nature* **1992**, *358*, 600–602.
6. Huang, L. R.; Tegenfeldt, J. O.; Kraeft, J. J.; Sturm, J. C.; Austin, R. H.; Cox, E. C. A DNA Prism for High-Speed Continuous Fractionation of Large DNA Molecules. *Nat. Biotechnol.* **2002**, *20*, 1048–1051.
7. Kaji, N.; Tezuka, Y.; Takamura, Y.; Ueda, M.; Nishimoto, T.; Nakanishi, H.; Horiike, Y.; Baba, Y. Separation of Long DNA Molecules by Quartz Nanopillar Chips under a Direct Current Electric Field. *Anal. Chem.* **2004**, *76*, 15–22.
8. Yasui, T.; Kaji, N.; Ogawa, R.; Hashioka, S.; Tokeshi, M.; Horiike, Y.; Baba, Y. DNA Separation by Square Patterned Nanopillar Chips. *Micro Total Anal. Syst. 2007* **2007**, *2*, 1207–1209.
9. Han, J.; Craighead, H. G. Separation of Long DNA Molecules in a Microfabricated Entropic Trap Array. *Science* **2000**, *288*, 1026–1029.
10. Fu, J.; Schoch, R. B.; Stevens, A. L.; Tannenbaum, S. R.; Han, J. A Patterned Anisotropic Nanofluidic Sieving Structure for Continuous-Flow Separation of DNA and Proteins. *Nat. Nanotechnol.* **2007**, *2*, 121–128.
11. Mao, P.; Han, J. Massively-Parallel Ultra-High-Aspect-Ratio Nanochannels as Mesoporous Membranes. *Lab Chip* **2009**, *9*, 586–591.
12. Fu, J.; Yoo, J.; Han, J. Molecular Sieving in Periodic Free-Energy Landscapes Created by Patterned Nanofilter Arrays. *Phys. Rev. Lett.* **2006**, *97*, 018103.
13. Li, W. L.; Tegenfeldt, J. O.; Chen, L.; Austin, R. H.; Chou, S. Y.; Kohl, P. A.; Krotine, J.; Sturm, J. C. Sacrificial Polymers for Nanofluidic Channels in Biological Applications. *Nanotechnology* **2003**, *14*, 578–583.
14. Cross, J. D.; Strychalski, E. A.; Craighead, H. G. Size-Dependent DNA Mobility in Nanochannels. *J. Appl. Phys.* **2007**, *102*, 024701.
15. Pennathur, S.; Baldessari, F.; Santiago, J. G.; Kattah, M. G.; Steinman, J. B.; Utz, P. J. Free-Solution Oligonucleotide Separation in Nanoscale Channels. *Anal. Chem.* **2007**, *79*, 8316–8322.
16. Doyle, P. S.; Bibette, J.; Bancaud, A.; Viovy, J. L. Self-Assembled Magnetic Matrices for DNA Separation Chips. *Science* **2002**, *295*, 2237.
17. Tabuchi, M.; Ueda, M.; Kaji, N.; Yamasaki, Y.; Nagasaki, Y.; Yoshikawa, K.; Kataoka, K.; Baba, Y. Nanospheres for DNA Separation Chips. *Nat. Biotechnol.* **2004**, *22*, 337–340.
18. Zeng, Y.; He, M.; Harrison, D. J. Microfluidic Self-Patterning of Large-Scale Crystalline Nanoarrays for High-Throughput Continuous DNA Fractionation. *Angew. Chem., Int. Ed.* **2008**, *47*, 6388–6391.
19. Zeng, Y.; Harrison, D. J. Self-Assembled Colloidal Arrays as Three-Dimensional Nanofluidic Sieves for Separation of Biomolecules on Microchips. *Anal. Chem.* **2007**, *79*, 2289–2295.
20. Nazemifard, N.; Bhattacharjee, S.; Masliyah, J. H.; Harrison, D. J. DNA Dynamics in Nanoscale Confinement under Asymmetric Pulsed Field Electrophoresis. *Angew. Chem., Int. Ed.* **2010**, *49*, 3326–3329.
21. Slater, G. W.; Tessier, F.; Kopecka, K. The Electroosmotic Flow (EOF). *Methods Mol. Biol.* **2010**, *583*, 121–134.
22. Pu, Q. S.; Yun, J. S.; Temkin, H.; Liu, S. R. Ion-Enrichment and Ion-Depletion Effect of Nanochannel Structures. *Nano Lett.* **2004**, *4*, 1099–1103.
23. Stein, D.; Kruithof, M.; Dekker, C. Surface-Charge-Governed Ion Transport in Nanofluidic Channels. *Phys. Rev. Lett.* **2004**, *93*, 035901.
24. Kim, S. J.; Wang, Y. C.; Lee, J. H.; Jang, H.; Han, J. Concentration Polarization and Nonlinear Electrokinetic Flow near a Nanofluidic Channel. *Phys. Rev. Lett.* **2007**, *99*, 044501.
25. Kaji, N.; Ogawa, R.; Oki, A.; Horiike, Y.; Tokeshi, M.; Baba, Y. Study of Water Properties in Nanospace. *Anal. Bioanal. Chem.* **2006**, *386*, 759–764.
26. Tsukahara, T.; Hibara, A.; Ikeda, Y.; Kitamori, T. NMR Study of Water Molecules Confined in Extended Nanospaces. *Angew. Chem., Int. Ed.* **2007**, *46*, 1180–1183.
27. Sakakibara, J.; Adrian, R. J. Whole Field Measurement of Temperature in Water Using Two-Color Laser Induced Fluorescence. *Exp. Fluids* **1999**, *26*, 7–15.
28. Chen, Y. Y.; Wood, A. W. Application of a Temperature-Dependent Fluorescent Dye (Rhodamine B) to the Measurement of Radiofrequency Radiation-Induced Temperature Changes in Biological Samples. *Bioelectromagnetics* **2009**, *30*, 583–590.
29. Ross, D.; Gaitan, M.; Locascio, L. E. Temperature Measurement in Microfluidic Systems Using a Temperature-Dependent Fluorescent Dye. *Anal. Chem.* **2001**, *73*, 4117–4123.
30. Paul, P. H.; Garguilo, M. G.; Rakestraw, D. J. Imaging of Pressure- and Electrokinetically Driven Flows through Open Capillaries. *Anal. Chem.* **1998**, *70*, 2459–2467.
31. Nagata, H.; Tabuchi, M.; Hirano, K.; Baba, Y. Microchip Electrophoretic Protein Separation Using Electroosmotic Flow Induced by Dynamic Sodium Dodecyl Sulfate-Coating of Uncoated Plastic Chips. *Electrophoresis* **2005**, *26*, 2247–2253.
32. Huang, X. H.; Gordon, M. J.; Zare, R. N. Current-Monitoring Method for Measuring the Electroosmotic Flow-Rate in Capillary Zone Electrophoresis. *Anal. Chem.* **1988**, *60*, 1837–1838.